CEAS Aeronautical Journal (2021) 12:331–344
https://doi.org/10.1007/s13272-021-00502-0

ORIGINAL PAPER

Investigation of biogenic materials and ferroelectrets for energy harvesting on vibrating aircraft structures

H. Holzmann[1] · M. Weber[2] · Y. J. Park[3] · S. Perfetto[3] · H. Atzrodt[3] · A. Dafnis[2]

Received: 4 May 2020 / Revised: 12 February 2021 / Accepted: 24 February 2021 / Published online: 27 March 2021

Abstract

In this publication the application of novel piezoelectric materials for energy harvesting on vibrating aircraft structures is investigated. These materials have significant advantages over conventional piezoelectric transducer materials like piezoceramics. In particular, biogenic materials in the form of wood-based materials and ferroelectrets in the form of irradiation cross-linked polypropylene are the subject of the investigation. The material characterization in terms of mechanical and electromechanical properties is shown for both material types. For the wood materials a compression test is used as the material has load-bearing properties. The ferroelectrets provide high compliances and are therefore investigated in a tensile test for material characterisation as well as in a four-point flexural test regarding its behaviour when glued to a dynamically bending surface. Additionally an FE-model of the material model for ferroelectrets is presented, which is validated by experimental results. An estimation of the power output is given for different concepts with both kinds of materials.

Keywords Energy harvesting · Aeronautics · Biogenic materials · Ferroelectrets · Piezoelectric effect

List of symbols

Roman symbols

A_{E}	Electrode surfaces
A_f	Force application surfaces
A_{Pol}	Polarization surface
A_{Ref}	The reference surface
$\boldsymbol{B}$	Damping matrix
D	Charge density
E	Electric field
f	Force
$\boldsymbol{K}$	Stiffness matrix
$\boldsymbol{M}$	Mass matrix
q	Charge
$\boldsymbol{S}$	Strain tensor
s_{ij}	Compliances
$\boldsymbol{T}$	Stress tensor
$\boldsymbol{x}$	Vector of deflections
$\boldsymbol{Y}$	Young's modulus

Greek symbols

δ_{ij}	Piezoelectric charge constants
ϵ_{ij}	Permittivities
ω	Frequency
ϕ	Voltage
ρ	Mass-density

✉ H. Holzmann
hendrik.holzmann@sam.tu-darmstadt.de

M. Weber
maximilian.weber@sla.rwth-aachen.de

[1] Research Group System Reliability, Adaptive Structures, and Machine Acoustics SAM, Technical University Darmstadt, Otto-Berndt-Str. 2, 64287 Darmstadt, Germany

[2] Institute of Structural Mechanics and Lightweight Design (SLA), RWTH Aachen University, Wüllnerstraße 7, 52062 Aachen, Germany

[3] Fraunhofer Institute for Structural Durability and System Reliability LBF, Bartningstraße 47, 64289 Darmstadt, Germany

1 Introduction

Climate change undoubtedly represents one of the main challenges of human kind of the current and future centuries. The still growing world population with a simultaneous striving of wealth including mobility for more and more people requires new technological innovations and a fundamental change in infrastructure and human habits. In 2016 air traffic caused 2.8% of carbon dioxide emissions [1], a number that could rise in case of a very likely increase of flight passengers around the globe. More ecologically friendly air traffic will be a part of the solution. In every phase of

aircraft operation, lightweight structures are prone to vibrations, whose mechanical energy remains unused. Within the framework of the project EnerVib (Innovative Energy Generation Concepts from Vibrating Aircraft Structures) the research question is clarified how and to what extent the vibration energy can be converted into electrical energy effectively. The aim is to power microelectronics like sensors in difficultly accessible areas of aircraft. Thus cables with their associated weights can be reduced and eventually fuel can be saved. The investigation focuses in particular on biogenic materials and ferroelectrets, which are to be integrated into the aircraft as transducer materials for flat or freely oscillating Energy-Harvesters (EH). With a high eco-efficiency of wood materials and a high structural flexibility of ferroelectrets, these materials have significant advantages over conventional piezoelectric materials. As an example of an aircraft-component a wingbox (cf. Fig. 1) is chosen providing cyclic deformations in the form of vibrations for Energy Harvesting with both material kinds. In Holzmann et al. [2] it is shown that realistic strain magnitudes can be calculated to around $4.5 \cdot 10^{-5}$ m $\cdot$ m^{-1} at a frequency of around 1.5 Hz.

Due to its load-bearing properties piezoelectric wood materials can be integrated directly into the flux of forces, replacing material of the wing structure e.g. of ribs, stringers, struts or cross beams. To ensure stability of the mechanical structure, sandwich-arrangements of wood and metals are a possible solution. Ferroelectrets on the other hand are highly compliant materials that can be attached to large surfaces of the structure using local surface strains for energy conversion. Therefore ferroelectrets are passively applied to the structure in parallel to the force flux. Because of the difference in application, different kinds of experiments are conducted for the two material types in this work.

1.1 Piezoelectric constitutive equations

The material characterisation and numerical simulation in the following investigations of piezoelectric wood-based materials and ferroelectrets are based on physical fundamentals. The piezoelectric properties are coupled with the mechanical properties via the piezoelectric constitutive equations

$$\boldsymbol{S} = \boldsymbol{s}^{\boldsymbol{E}}\boldsymbol{T} + \boldsymbol{\delta}\boldsymbol{E} \tag{1}$$

and

$$\boldsymbol{D} = \boldsymbol{\delta}\boldsymbol{T} + \boldsymbol{\epsilon}^{\boldsymbol{T}}\boldsymbol{E} \tag{2}$$

with compliances s_{ij}, piezoelectric charge constants δ_{ij} and permittivities ϵ_{ij}. $\boldsymbol{S}$ is the strain tensor, $\boldsymbol{T}$ the stress tensor, $\boldsymbol{E}$ the electric field and $\boldsymbol{D}$ the electric charge density. For sufficiently small surface elements, the electric field can be considered constant and the piezoelectric material can be approximated through a plate capacitor. For a constant electric field $E = 0$ Eq. 2 is simplified to

$$D = \delta T. \tag{3}$$

By including

$$D = \frac{q}{A_{\mathrm{E}}} \tag{4}$$

with the charge q and the assumption that the specimen is regarded as a plate capacitor with the electrode and force application surfaces A_{E} and A_f the equation can be transformed to

$$\delta = \frac{q}{f}\frac{A_f}{A_{\mathrm{E}}} \tag{5}$$

with the force f as axial load. For an alternating current as the output of a harmonically excited piezoelectric material with the frequency ω, the power output can be expressed as

$$P_{\mathrm{el}} = \frac{u_{\mathrm{el}}^2}{2 \cdot R_{opt}} = u_{\mathrm{el,eff}}^2 \cdot \omega \cdot C \tag{6}$$

with the electrical voltage u_{el}, optimal load resistance $R_{\mathrm{opt}} = \omega \cdot C$, the frequency ω and the capacitance of the piezoelectric transducer C. Using the piezoelectric constitutive equations with open electrodes ($D = 0$) and by eliminating u_{el} the power output subject to a strain excitation S can be expressed as

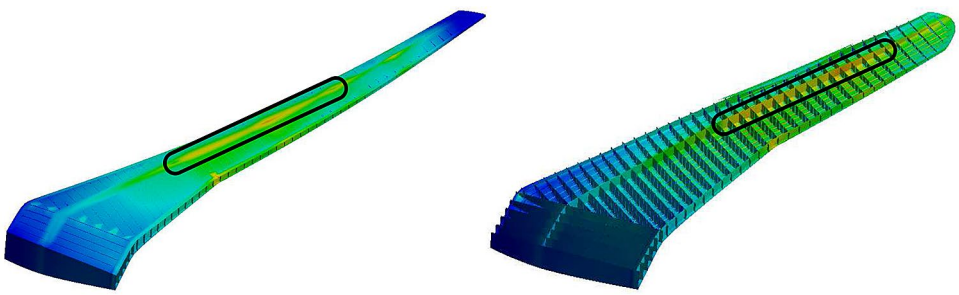

Fig. 1 Simulated qualitative strain in the first vibration mode of the NASA Common Research Model wingbox structure (blue: min., red: max.) [3]. Potential areas for Energy Harvesting with ferroelectrets on structure surfaces (left) and with wood materials integrated into the structure shown in the cross-section (right)

$$P_{\mathrm{el}} = \frac{\delta^2 Y^2 A_{\mathrm{piezo}} t_{\mathrm{piezo}}}{2\epsilon} \cdot \omega \cdot S^2 \tag{7}$$

with the Young's modulus Y, the surface Area A_{piezo} of the transducer electrode and the thickness t_{piezo}.

1.2 Wood materials

Due to its chemical and mechanical properties, wood is applied in the most diverse areas. As a natural and renewable raw material it is used for energetic purposes as well as a construction material. Because of its specific strength and rigidity the fibre composite material comes into effect in lightweight design for load-bearing structures. In addition, wood has good fatigue strength and a fail-safe character. Furthermore, wood has piezoelectric properties, which were first discovered in the 1940s and are still the subject of current research activities [4].

Figure 2 shows the schematic cell structure of cellulose. The piezoelectric effect is made possible by a crystalline structure, which consists of different cell layers. If shear stresses are induced into the structure, a displacement of charge centres occurs, which results in electric dipole moments and a polarization. Its magnitude depends on the applied load and on the parameters of the wood itself, which are mainly limited to the type of wood, humidity and temperature. The piezoelectric charge constant δ of Eq. 5 can be used as a characteristic value for the conversion of

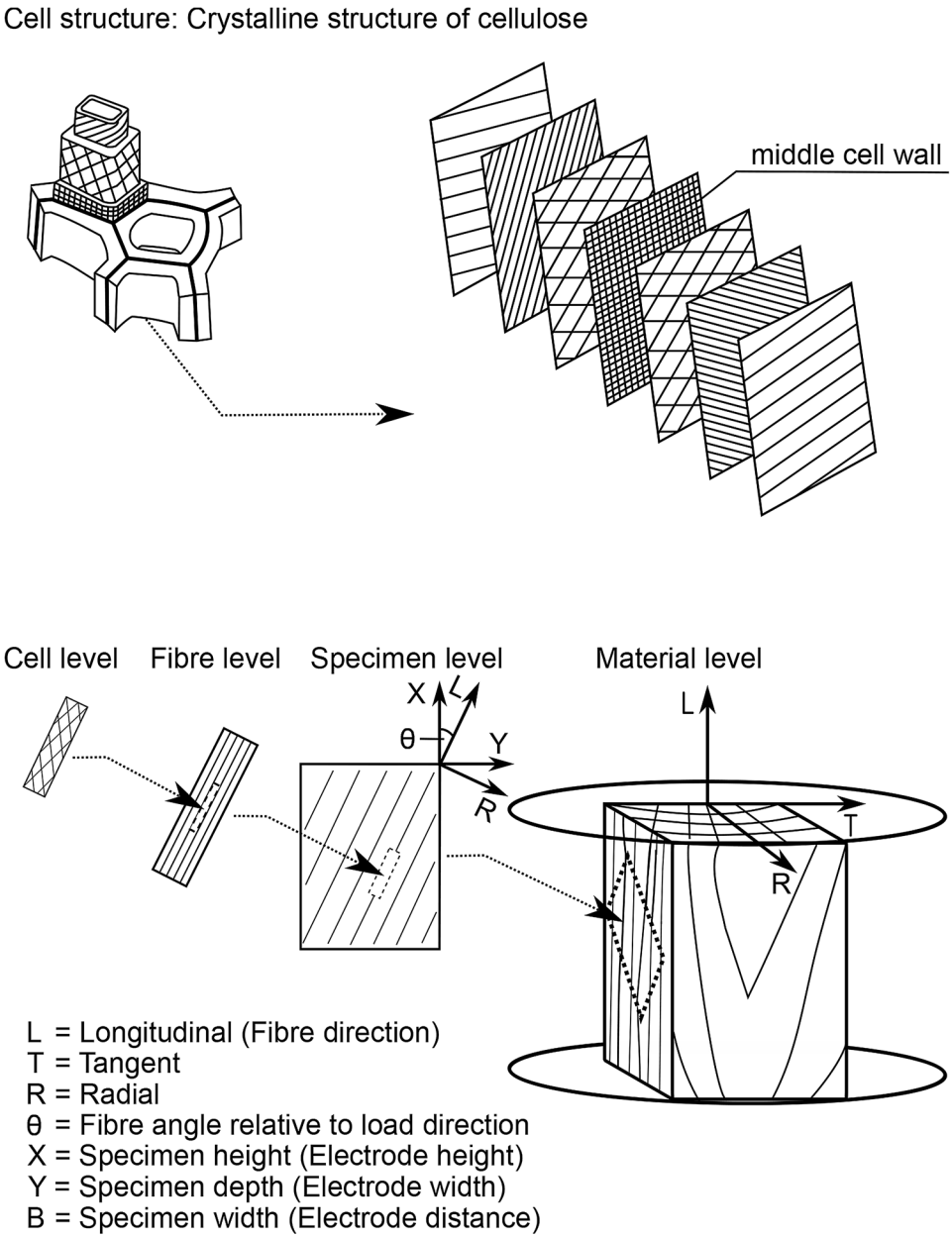

Fig. 2 Cell structure, sample and material level of wood-based materials

mechanical force into electric charge. For wood, the charge constant δ is in the order of 5% of that of quartz crystals [5]. In a direct comparison of the transducer characteristics of wood to piezo crystals and especially to modern piezoceramics (Table 4), piezoceramics exceed wood materials. In addition, the low piezoelectric charge constant of wood complicates energy harvesting, because the low currents must first cover the power loss of the energy processing before any electrical energy can be stored and used by consumers. But to compensate for this problem, the wood offers a significant advantage over conventional piezo materials. Due to its mechanical properties, large volumes of the transducer material can be integrated. The aim is to substitute the existing structures with piezoelectric load-bearing structures. This substitution can occur without significant weight increase, as shown in Fig. 3 for aluminium.

A beam cross-section made of aluminium, which is used as a reference is compared to three selected cross-sections with the same bending stiffness. In option one, a cross-section is shown that must have the same height as the reference due to the construction space, but is made wider. The cross-section of Wood Beam 1 has a mass increase of 20 percent compared to the aluminium cross-section. In the case where there are no limits on size, the aluminium cross-section can be substituted without an increase in mass by using Wood Beam 2. The third option with enormous lightweight potential is the composite beam. If there are construction space limitations, a cross-section can be designed from a variable composite of several materials. In this example, 25 percent of the width of the aluminium of the reference cross-section was substituted by wood. The increase in mass is only five percent. This offers a realistic potential for integrating the piezoelectric properties of the wood.

The production process of wood-based energy harvesters brings further advantages. While piezoceramics are time-consuming and thus cost-intensive to produce, certain production steps, such as the polarization imprinting after the sintering process, are not required for wood-based materials. In addition to economic advantages, wood is a renewable and eco-friendly material. Its environmental friendliness results from its sustainable regeneration and good recyclability. At the Institute of Structural Mechanics and Lightweight Design (SLA) at RWTH Aachen University multifunctional structures and mechanisms are developed, which combine the advantages of wood-based materials and thus create a pioneering concept of energy harvesting.

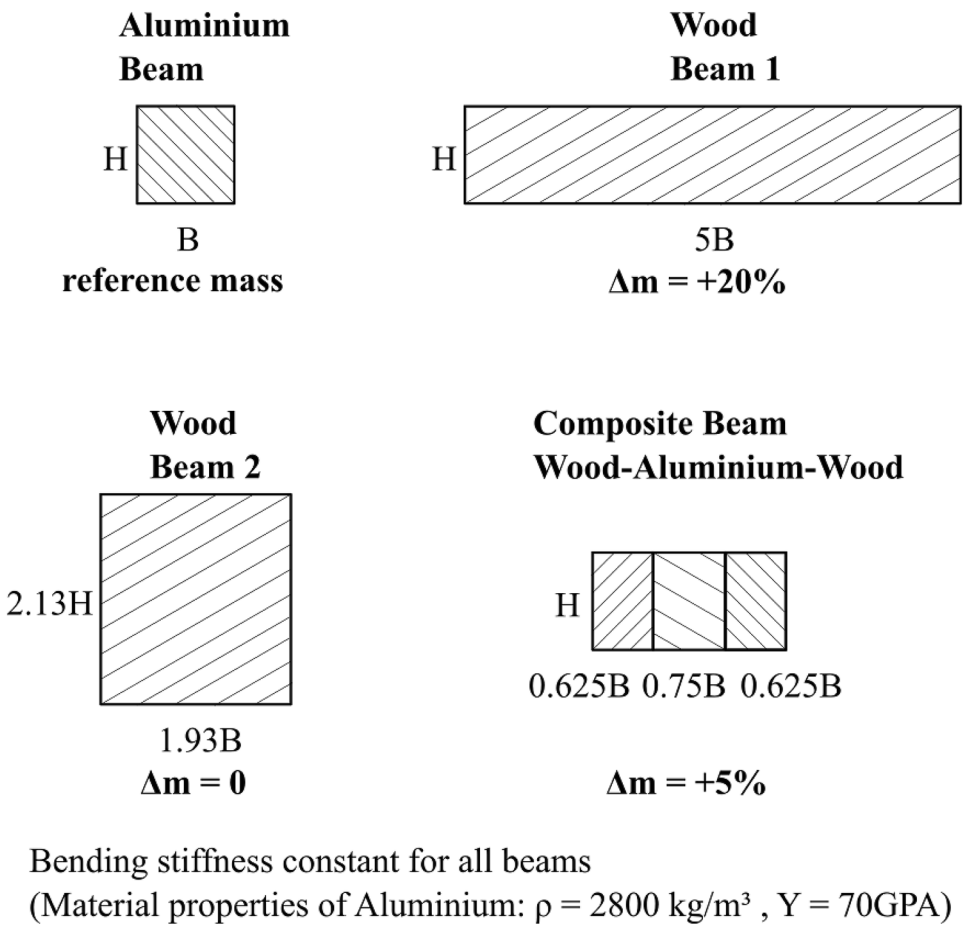

Fig. 3 Different possibilities for substituting aluminium with wood

Figure 4 illustrates two basic conceptual approaches. On the one hand, flat, integrative structures are developed that combine the strength, stiffness and piezoelectric properties of wood. The focus is on ribs, skin panels, stringer profiles, struts and cross beams. Hybrid materials have a laminate structure of fibre composite materials and the transducer layers of wood incorporated into the supporting structure, which are idealized as a disk. A further side effect is the increase in intrinsic material damping due to the possible conversion of deformation energy into thermal energy. In addition to multifunctional structures, the development of absorber mechanisms is a major motivation. These are frequency-tuned, cantilever-resonators which are applied to vibrating structures. Vibrations are induced into the absorber masses by base excitations, which lead to excessive amplitudes at the resonance frequencies. The spring elements, which form the connection of the absorber mass and the base point, are made of piezoelectric material. With these two concepts, a wide range of vibrations can be used to convert mechanical energy into electrical energy in aircraft-structures. The possibility of passive vibration suppression with the multifunctional structures and mechanisms creates a double-use. Moreover, the increase in structural durability and the reduction of acoustic vibrations have further synergistic effects that qualify the use of wood-based materials as a transducer material. As mentioned above, the tests conducted in this work focus the first of the two concepts.

1.3 Ferroelectrets

In addition modern ferroelectrets represented by irradiation cross-linked polypropylene (IXPP) are investigated. Due to high piezoelectric transducer coefficients and high structural flexibility, these electromechanical transducer materials combine the advantages of piezoceramics and electroactive polymers. Electrets provide a permanent electric field caused by a forced charge separation in the material itself. This charge separation can be induced by a so-called corona charging, leading to an electrical breakdown in the dielectric. Through metallic electrodes vaporized onto the material, compensation charges appear when connected to an electrical circuit. Through a cyclic deformation of the material, the electric field changes periodically and hence the compensation charges can be used as an alternating electric current. The electret-material has gained piezoelectric properties and is therefore called piezo- of ferroelectret. In Fig. 5 two types of ferroelectrets are shown, that are investigated in the Research group System Reliability, Adaptive Structures, and Machine Acoustics (SAM).

One type is irradiated cross-linked polypropylene (IXPP) as shown on the left. It provides an increased temperature stability of the piezoelectric transducer coefficients compared to regular polypropylene ferroelectrets achieved by a radiation process of the foam material. A hot-pressing process reduces the thickness and increases the compliance of the material in thickness-direction at the same time. After the corona charging process electric surface-charges emerge on the voids of the foam, that cause a quasi-permanent electric field [8]. IXPP is mostly used as a δ_{33}-transducer. However, the material also works in the 31-mode. IXPP usually provides δ_{33}-constants in the range from 300 up to 700 pC/N being in the same order of magnitude as piezoceramics. The charge constants perpendicular to the polarization axis are about two orders of magnitude lower [9, 10]. Another type is parallel tunnel fluorethylenepropylene (FEP), having a macroscopic tunnel-structure, that is formed by a fusion of two waved layers of FEP. The structure is shown on the right-hand-side of Fig. 5. The tunnels work similar to the air-voids of the foams as macroscopic cavities separating the charges after corona charging. When the material is exposed to an external load perpendicular to the tunnels length axis, the tunnels deform and an electric potential can be measured between the electrodes. Parallel-tunnel FEP is designed as a d_{31}-transducer despite having high δ_{33} -constants of about 1300 pC/N as well [9]. Ferroelectrets are a subject of research for Energy Harvesting only since

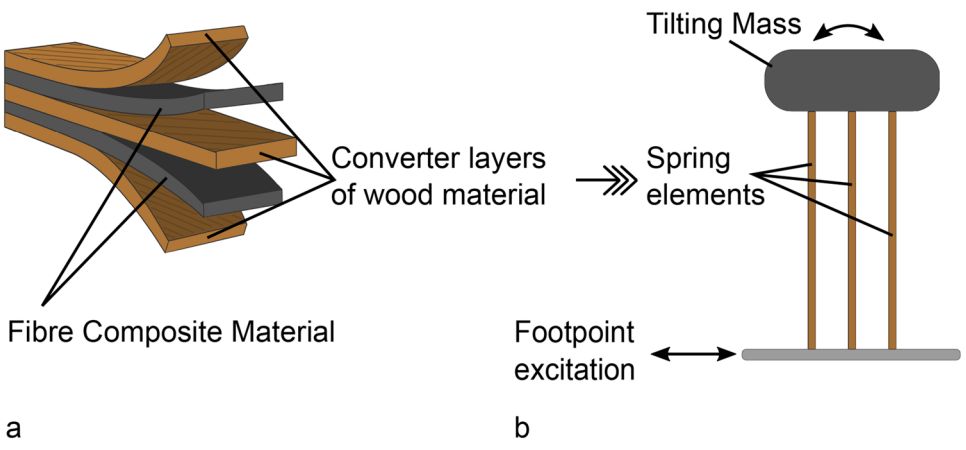

Fig. 4 Conceptual approaches: **a** multifunctional structure, **b** tilting mechanism as resonator

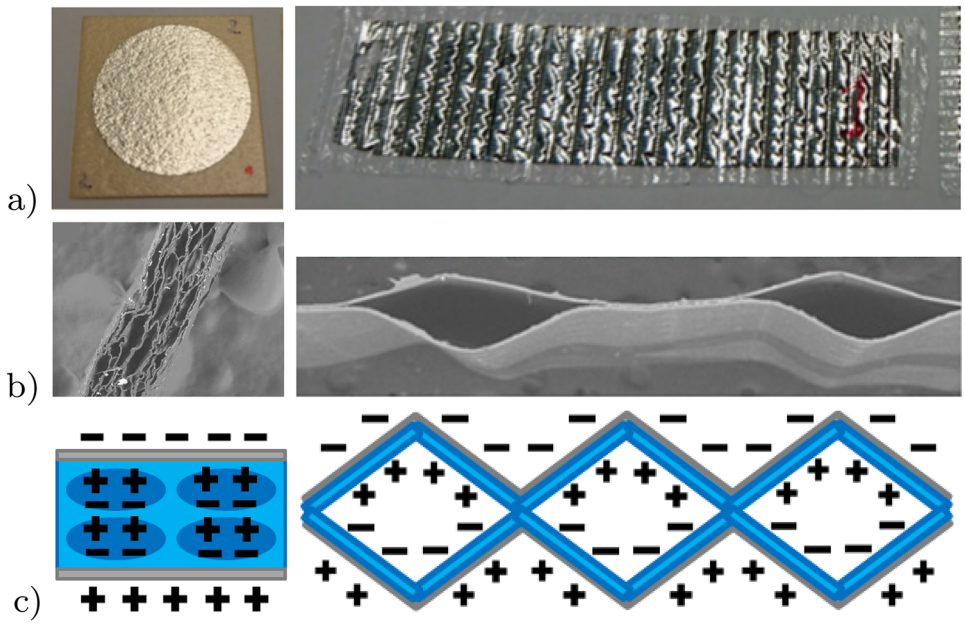

Fig. 5 Ferroelectrets, left: IXPP, right: parallel-tunnel FEP, **a** photos, **b** microstructure in thickness direction [6, 7], **c** schematic structure in thickness direction with charge distribution

2012 and provide a huge potential for the use in lightweight-structures. Analytical models for the electrical power-output of ferroelectret-EH have been developed by Pondrom for harvesters working in both the δ_{33} and δ_{31}-mode [11]. These models describe systems with one degree of freedom including a seismic mass. The systems are optimized for a certain frequency. Regarding ferroelectrets the project addresses the question of research, if and to what extend distributed EH based on ferroelectrets can be used in a wide frequency range. This work focuses on the ferroelectret IXPP, due to the fact that it can be produced in larger sheets and that it is more robust than parallel-tunnel FEP.

2 Investigation of piezoelectric wood-based materials

There are various investigations on the piezoelectric behaviour of wood-based materials. These include the most diverse types of wood, which have, however, been insufficiently investigated with regard to major influential parameters such as humidity and temperature. The results show significant deviations and also contradictions. Therefore, only few conclusions can be derived to select a suitable wood type as transducer material. Specific values characterizing the performance must therefore be determined. In the course of this problematic, an extensive material characterization is carried out to determine the electro-mechanical properties of different biogenic transducer materials. To measure the piezoelectric effect in wood-based materials, a test setup is designed and verified. As a fundamental for the characterization of the electro-mechanical properties of different biogenic transducer materials, the piezoelectric effect is first metrologically registered on a wooden cuboid and the results are compared with the literature references. Thus, the general test setup including the measurement chain are verified.

2.1 Material characterization

Figure 6 shows the general test setup with specimen, insulation, testing machine and charging cable. Currently there are no normative specifications defined. Hence the wooden cuboid is selected as a simple specimen geometry which can be regarded as a plate capacitor. First, the specimen is milled out of a solid wood block perpendicular to the LR plane at a grain angle of $\theta = 45°$ (see Fig. 2). With axial load in the X or Y direction, the greatest possible shear is thus obtained and the piezoelectric effect is at its maximum. A conductive bronze coating is applied to the two surfaces in the LR plane, forming the electrodes. According to theory, they are polarized and thus referred to as polarization surfaces in the following. Electric plugs are attached to this coating with silver conductive adhesive, to which the highly insulated charge cable is connected. Investigations of various insulation materials have shown that plastics such as the highly insulating Teflon are particularly unsuitable for insulating samples and specimen holders, since static charging of these materials is accompanied by changes in the electrical field, so that the piezoelectric effect can no longer be differentiated from these disturbances. Glass ceramic plates (Macor) do not show this effect and are therefore chosen for the insulation between specimen and the specimen holder of the hydraulic testing machine type SCHENK POZ 160. This machine applies a cyclical pressure load to the specimen.

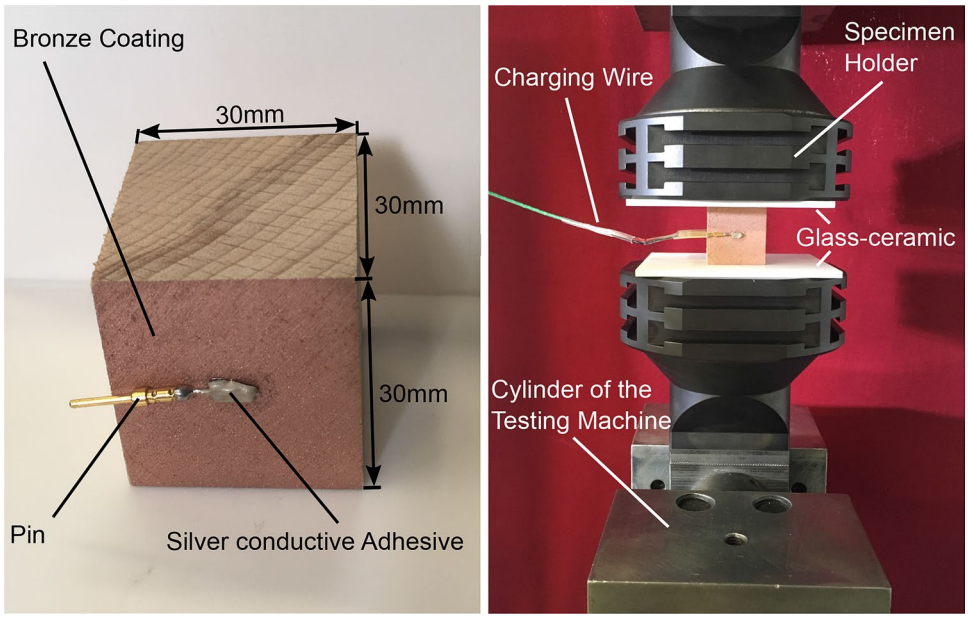

Fig. 6 Test setup, on the left: sample with coating and pins, on the right: total setup

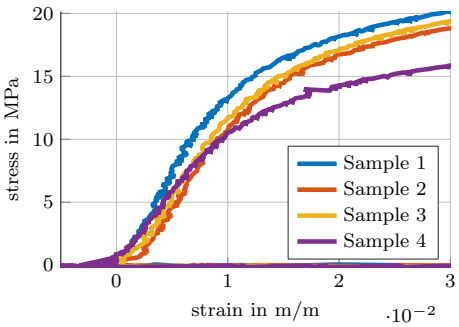

Fig. 7 Measurement graphs of stress over strain for a compression test of wood materials

Table 1 Young's modulus of the tested samples and average $\overline{Y}$

Sample ID	Young's modulus in MPa
1	1564
2	1365
3	1368
4	1039
$\overline{Y}$	**1334**

To be able to measure the charges applied to the electrodes, a charge amplifier type KISTLER 5015 is connected to the cables.

To determine material parameters compression tests were performed on wood samples with a grain angle of 45° to the direction of loading. From these tests, a Young's modulus of 1334 MPa and a yield strength of 12.2 MPa were determined as mechanical parameters. The stress-strain graphs are shown in Fig. 7 with their respective values for the Young's modulus in Table 1.

2.2 Comparison of theoretical polarization surface and reference surface

For this comparison, a cuboid of European beech with a wood moisture content of 8% with four identical electrode surfaces is investigated. Two electrodes were applied to the polarization surfaces and two to reference surfaces perpendicular to them. The two samples were subjected to a swelling pressure load of the form

$$f = f_0 + \hat{f}\sin((2\pi\omega)t) \tag{8}$$

with $f_0 = 1$ kN, $\omega = 2$ Hz and $\hat{f} = 0.25$ kN. The test setup with the specimen is shown in Fig. 8.

Figure 9 shows the graphs of charge and force for the polarization surface A_{Pol} and the reference surface A_{Ref}. Both surfaces have a sinusoidal charge curve that follows the force curve. There are significant differences between the maximum amplitudes of the charge lines. As described theoretically, the polarizations occur at the expected surfaces. At the same time, there are also charge changes at the reference surfaces that can be measured.

2.3 Comparison of 0° and 45° grain to load direction

For this comparison, two cubes made of European beech with a wood moisture content of 8% and edge lengths of 30mm are investigated. The grain directions were differentiated between $\theta = 0°$ and $\theta = 45°$. The cuboids were set under

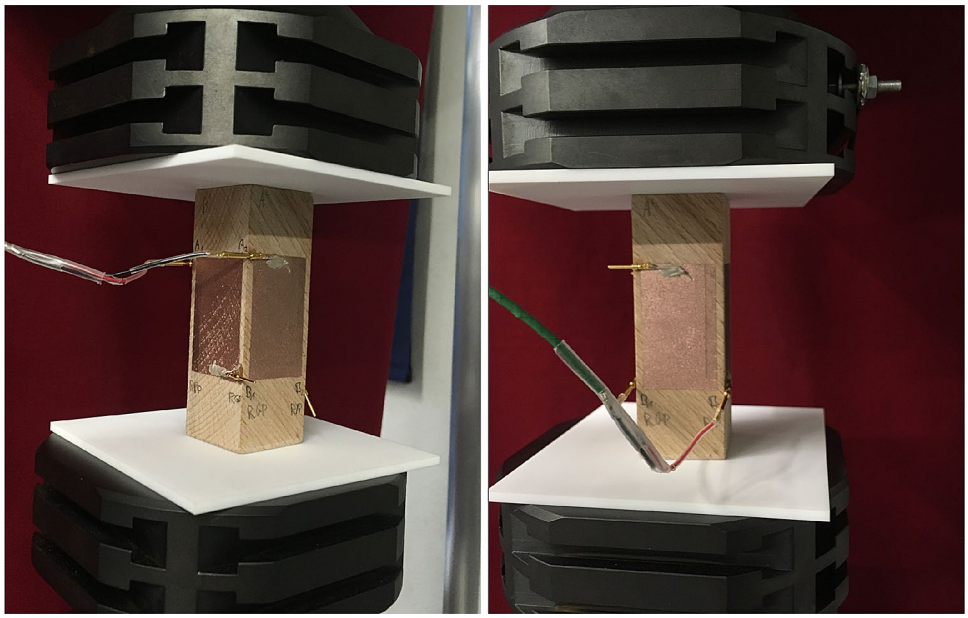

Fig. 8 Specimen with 4 electrode surfaces, on the left: theoretical polarization surfaces A_{Pol}, on the right: reference surfaces A_{Ref}

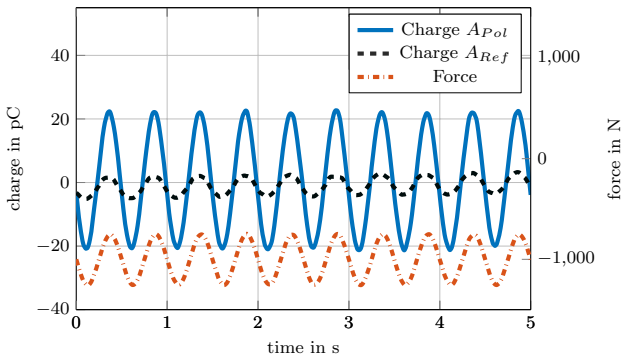

Fig. 9 Charge and force (red) curves of polarization (blue) and reference surfaces (black) in comparison

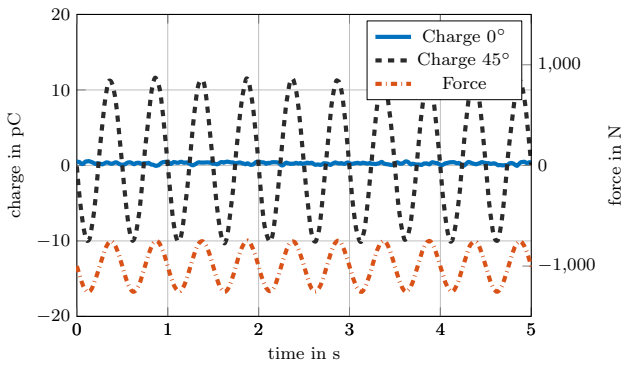

Fig. 10 Charge and force (red) curves of 0° (blue) and 45° (black) specimens in comparison

the same pressure load as the cube in Sect. 2.2. Under this load, no piezoelectric effect is expected to be registered in the 0° due to the absence of shear stress, which is a premise for the polarization of the electrodes. On the other hand, a sinusoidal load curve is expected for the 45°-specimen with a sinusoidal force curve.

Figure 10 shows the curves of charge and force for the 0° and 45° samples. As expected, the 0° specimen does not feature a piezoelectric effect. The 45°-specimen shows a sinusoidal charge curve that follows the force curve. According to Eq. 5 the piezoelectric charge constant δ is calculated to be 0.044 pC/N and is thus in the range from 0.037 to 2.3 pC/N given in the literature [5, 12]. Compared to typical piezoelectric materials (Table 4) the piezoelectric properties of wood are significantly lower. Despite this, the following example demonstrates the potential for using this material as an energy harvester.Integrating wood with a mass of 1 kg and a thickness of 5mm, under ideal load conditions with the assumptions of a frequency of 1.5 Hz at a strain of $4.5 \cdot 10^{-5}$ m $\cdot$ m^{-1} an electrical energy of 2.37 nW can be achieved according to Eq. 7. Through applied lightweight design, this quantity can be expanded without significant weight increase and thus wood gains more importance as an energy harvester.

3 Investigation of ferroelectrets

The application and experimental investigation of ferroelectrets on real aircraft-structures is costly and can be problematic considering safety standards. Therefore the focus is the experimental investigation of simplified structures with EH and especially the simulation of these. Due to the fact that aircraft-structures have curved surfaces, analytical models as the ones by Pondrom [11] are neglected for the simulation

of the system. Instead a numerical modelling approach is pursued. For the latter one, first a material model of the ferroelectret IXPP is defined and in the next step the system investigated in this work is outlined. Moreover the experimental setup is described and the validation of the model with experimental data is presented.

3.1 IXPP material model

For the simulation of the material a linear model is used, because small local strains of aircraft base structures are assumed to affect the material. This assumption seems reasonable, as polymer foams show a linear elastic behaviour for small deflections [13]. In Fig. 11 a unit cell of the material is shown with a local coordinate system.

The coordinates 1 and 2 represent in-plane directions, the number 3 the direction of polarisation perpendicular to the 1- and 2- direction. Based on the literature [14] and the manufacturing process it is assumed, that the parameters in 1- and 2-direction are in the same order of magnitude so they are assumed identical. The parameters in 3-direction have different values. Hence, a linear transverse isotropic material model is chosen in this work. The parameters are included in Eq. 1 by means of compliances s_{ij}, piezoelectric charge constants δ_{ij} and permittivities ϵ_{ij}. Additionally to the mass-density ρ, the equations are imported into a commercial numerical simulation software. Viscoelastic and non-linear effects are neglected in this work.

3.2 Material characterization

To determine all relevant material properties from Sect. 3.1, measurements on several IXPP-samples are used aside manufacturer data. With a capacitance measurement the static capacitance of the samples is determined. For samples with a size of 60 by 60 mm^2 an average capacitance of 302.4 pF results with a standard deviation of 27.69%. Since a planar attachment of the ferroelectrets without a seismic mass to a vibrating structure primarily leads to a deformation of the ferroelectret in the directions 1 and 2, the derivation of the Young's modulus in 3-direction is not described at this point. Typical values are 0.54 [14] to 1.1 MPa [10]. By a tensile test the Young's modulus in plane direction is measured, as shown in Fig. 12. For this purpose four samples without electrode are tested with a given strain amplitude.

Using the slope of the graphs, the Young's modulus can be calculated to 133.3 N/m^2 in average as shown in Table 2. Furthermore a tensile test of an electroded specimen is conducted. After prestressing the specimen a force amplitude of $\hat{f} = 5$ N and a frequency of $\omega = 2$ Hz are applied. For the charge measurements, a laboratory charge amplifier was used that ensures the absence of any load-resistance by very

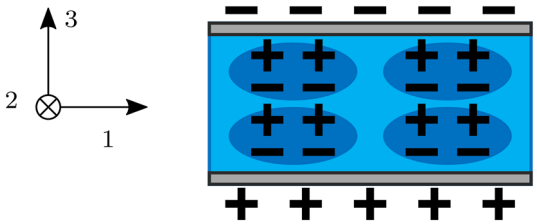

Fig. 11 Unit cell of the IXPP-ferroelectret with corresponding coordinates

Table 2 Young's modulus of the tested samples and average

Sample ID	Young's modulus in MPa
1	128.2
2	122.4
3	154.8
4	127.6
$\overline{Y}$	**133.3**

Fig. 12 Tensile test-rig for the determination of Young's Modulus in 1-direction (left) and measurement graphs of stress over strain (right)

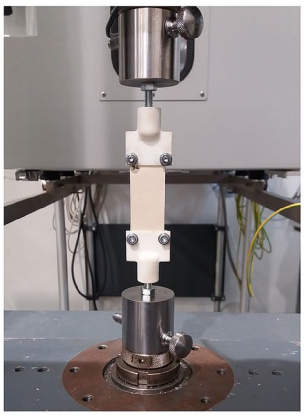

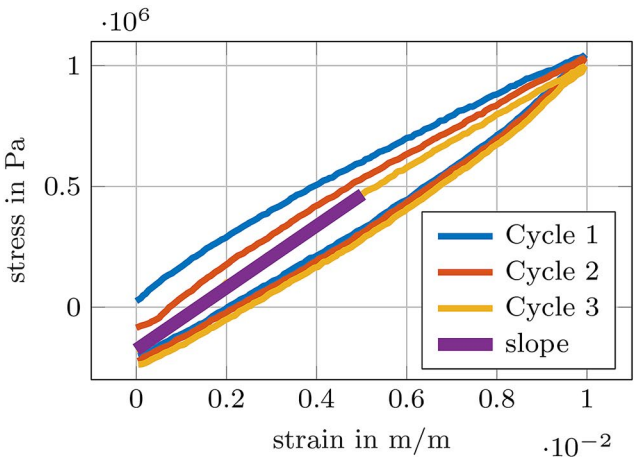

high input impedance. According to the charge amplifier principle, the generated charge is defined by the negative feedback capacitor (This also applies to the charge measurements for the investigated wood materials). The corresponding graph is shown in Fig. 13. The average charge amplitude is determined as 372.3 pC. Using Eq. 5 the piezoelectric charge constant δ_{31} is further calculated as 0.252 pC/N. As mentioned in Sect. 1.3, the investigated IXPP-ferroelectret is designed for the use in its 33-mode.

3.3 Four-point flexural test

In the case of a planar attachment of the ferroelectrets onto aircraft-components, surface strains of the vibrating structure are transferred directly to the ferroelectret-EH. Due to the much lower stiffness and density of the polymer compared to materials in aircraft like Aluminium or CFRP, the mechanical stiffness- and mass-properties of the aircraft-structure stay approximately the same. In a four-point flexural test the behaviour of IXPP-ferroelectrets glued to Aluminium-plates is investigated like outlined in Fig. 14. The force f acts as a symmetric excitation on both ends of the plate. The aluminium plate is pressed symmetrically at two rotatable bearings with its upper side.

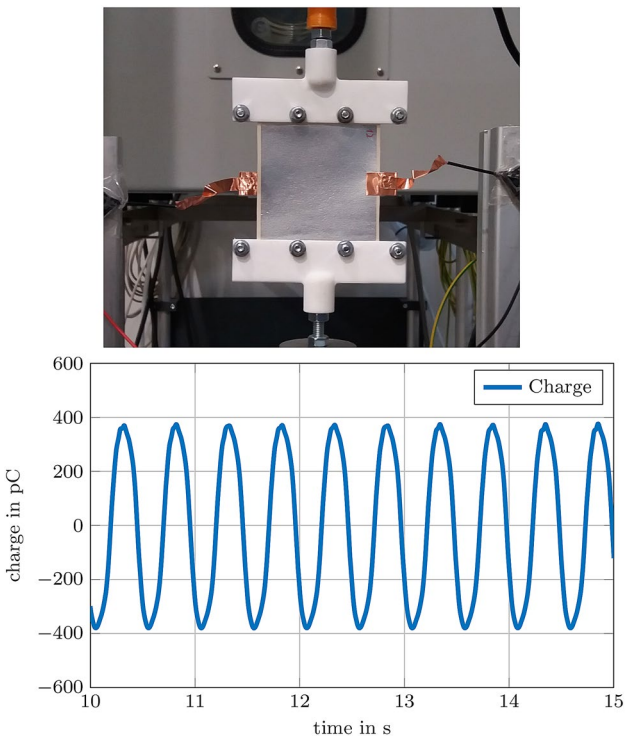

Fig. 13 Generated charge (bottom) by an IXPP-sample in the tensile test-rig (top) loaded with a sinusoidal force with amplitude of $\hat{f} = 5$ N and a frequency of $\omega = 2$ Hz after prestressing

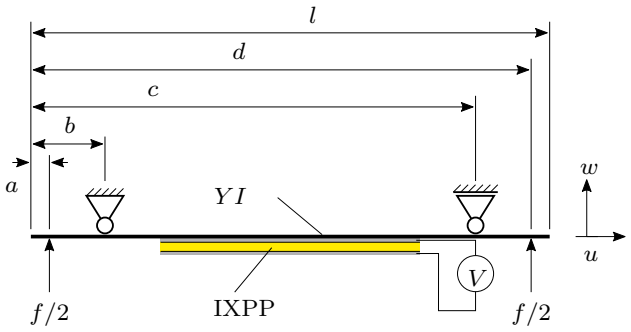

Fig. 14 Schematic four-point flexural test with ferroelectret and voltage-measurement (thickness of IXPP not to scale)

By design a constant momentum is caused in the sample holder by the application of the force f between the bearings and therefore a constant curvature and surface strain is achieved. When the plate and herewith the IXPP-sample is exposed to a load, the resulting electric voltage at the electrodes is measured.

The dimensions of the sample holder are adapted to the tested sample size with an edge length of 60 mm. The constants for the experimental setup are shown in Table 3. For a preliminary design the maximum force is calculated with a bending line. The parameters in Fig. 14 are specified as $a = 0,005$ m, $b = 0,2$ m, $c = 0,12$ m and $d = 0,135$ m due to design reasons. The equation for the momentum in the sample holder is

$$M(u) = YIw(u)'' = f(\langle u-a\rangle - \langle u-b\rangle - \langle u-c\rangle + \langle u-d\rangle). \tag{9}$$

Two-time integration leads to the bending line with

$$w(u) = \left[\frac{f}{6}(\langle u-a\rangle^3 - \langle u-b\rangle^3 - \langle u-c\rangle^3 + \langle u-d\rangle^3) + C_1 u + C_2\right]/YI. \tag{10}$$

Table 3 Constants of the flexural test

Sym.	Description	Value	Unit
l	Plate length	0.14	m
e	Plate width	0.11	m
t	Plate thickness	0.001	m
Y	Young's modulus of plate	$71 \cdot 10^9$	Pa
I	Geom. moment of inertia	$9.17 \cdot 10^{-12}$	m^4
a_{ixpp}	IXPP edge length	0.06	m
t_{ixpp}	IXPP thickness	$1.8 \cdot 10^{-4}$	m
C_{ixpp}	IXPP capacitance	384.29	pF

The constants can be derived from the boundary conditions $w(b) = w(c) = 0$ as

$$C_1 = \frac{f}{6(c-b)}\left((b-a)^3 + (c-b)^3 - (c-a)^3\right) \tag{11}$$

and

$$C_2 = -C_1 b - (f/6)(b-a)^3. \tag{12}$$

By means of the bending line, the maximum deflection of the sample holder exposed to the force f can be estimated. Taking a yield strength of 100 MPa the maximum force not leading to a plastic deformation of the aluminium structure of 1 mm thickness is calculated as 244.5 N. The corresponding maximum deflection and surface strain of the plate are −3.522 mm and 0.141% respectively. The emerging surface strain through a force of 1 N is calculated to $5.767 \cdot 10^{-4}$%.

3.3.1 Finite element model

With the system shown in Fig. 14, a finite element (FE) model is developed based on the geometry data in Table 3 discretization the aluminium plate and the IXPP-ferroelectret by means of hexahedric elements. The equation of motion for the mechanical system can be expressed in its most general form as

$$\boldsymbol{M}\ddot{\boldsymbol{x}} + \boldsymbol{B}\dot{\boldsymbol{x}} + \boldsymbol{K}_{xx}\boldsymbol{x} = \boldsymbol{f}(t), \tag{13}$$

with the mass matrix $\boldsymbol{M}$, the damping matrix $\boldsymbol{B}$, the mechanical stiffness matrix $\boldsymbol{K}_{xx}$, the vector of deflections $\boldsymbol{x} = [u\ v\ w]^{\mathrm{T}}$ and the external force vector $\boldsymbol{f}(t)$. Expanding the system by additional degrees of freedom $\boldsymbol{\phi}$ for the electric potential on all nodes of the piezoelectric material, the system of equations

$$\begin{bmatrix} \boldsymbol{M} & \boldsymbol{0} \\ \boldsymbol{0} & \boldsymbol{0} \end{bmatrix} \begin{bmatrix} \ddot{\boldsymbol{x}} \\ \ddot{\boldsymbol{\phi}} \end{bmatrix} + \begin{bmatrix} \boldsymbol{B} & \boldsymbol{0} \\ \boldsymbol{0} & \boldsymbol{0} \end{bmatrix} \begin{bmatrix} \dot{\boldsymbol{x}} \\ \dot{\boldsymbol{\phi}} \end{bmatrix} + \begin{bmatrix} \boldsymbol{K}_{xx} & \boldsymbol{K}_{x\phi} \\ \boldsymbol{K}'_{x\phi} & \boldsymbol{K}_{\phi\phi} \end{bmatrix} \begin{bmatrix} \boldsymbol{x} \\ \boldsymbol{\phi} \end{bmatrix} = \begin{bmatrix} \boldsymbol{f}(t) \\ \boldsymbol{q}(t) \end{bmatrix} \tag{14}$$

results. $\boldsymbol{K}_{x\phi}(\boldsymbol{\delta})$ is the piezoelectric coupling matrix, $\boldsymbol{K}_{\phi\phi}(\boldsymbol{\epsilon})$ the electric stiffness matrix and $\boldsymbol{q}(t)$ the vector of external charges applied to the electrical degrees of freedom [15, p. 32]. The system matrices represent an FE model derived from a volume model. The IXPP-properties are defined by the material model from Sect. 3.1. The force excitation is induced with the help of an external point, coupling all degrees of freedom of the edges of excitation. Additional mass is added to the edges as a model parameter. The FE model regarding the generated voltage on the IXPP-electrodes is shown in Fig. 15 when exposed to a static force.

For the simulation in the frequency and time domain, the systems matrices are exported from ANSYS Mechanical to MATLAB with the AdaptroSim®-Toolbox developed at the Fraunhofer Institute for Structural Durability and System Reliability (LBF) in Darmstadt. In MATLAB a model reduction of the piezo-mechanical structure and a conversion to a state-space representation is conducted as described in [15, p. 77].

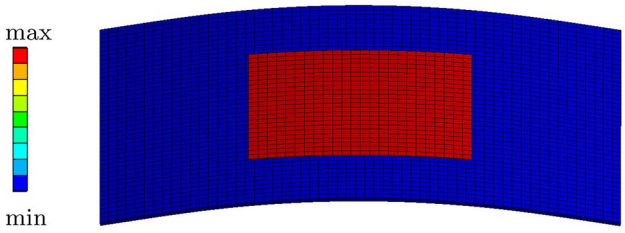

Fig. 15 Four-point flexural test represented by an ANSYS model: electric voltage caused by a static force applied to the edges of excitation

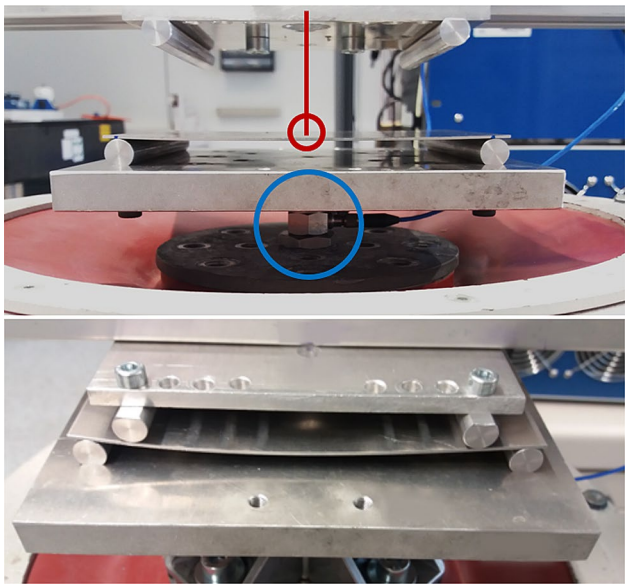

Fig. 16 Four-point flexural test, top: unloaded system (red: laser-measurement, blue: force and acceleration sensor), bottom: pre-stressed structure

3.3.2 Experimental validation

For the validation of the created model, an experimental setup is used as shown in Fig. 16 representing the system in Fig. 14. Aluminium-rolls are both used for the rotatable bearings and for the contact point for the induction of the shaker force. At the connection point between shaker and base plate, both force and acceleration can be measured.

In a first test, the electrical response of the electret in terms of voltage with open electrodes is measured when applying a static load to the setup shown in Fig. 16. For different forces the generated voltage is shown in Fig. 17.

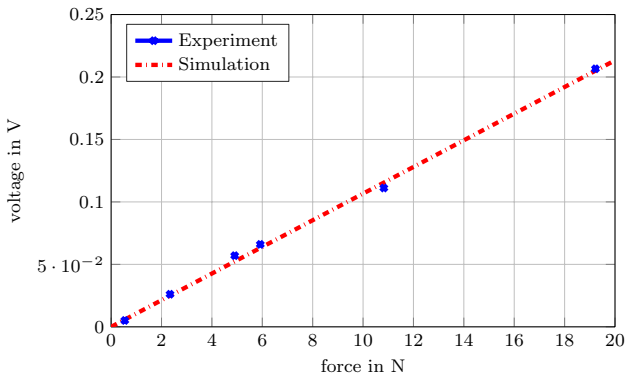

Fig. 17 Generated voltage between the IXPP-electrodes by static forces in the four-point flexural test setup

The simulated behaviour fits the experimental results in the investigated load range.

For the system identification, the transfer function of acceleration over excitation force

$$Z_{fa} = \frac{a(\omega)}{f(\omega)} \tag{15}$$

at the connection point is measured. Additionally the transfer function of the electrode voltage over excitation force

$$Z_{f\phi} = \frac{\phi(\omega)}{f(\omega)} \tag{16}$$

is identified. Both graphs are shown in Fig. 18 with their corresponding simulated behaviour.

A dominant resonance can be observed in both the mechanical and electrical transfer function, representing the first bending mode of the plate. A model fit is achieved by choosing a mass of 0.75 kg for the base plate of the setup and a structural damping of 3%. The damping matrix is implemented by a Rayleigh damping model. A good agreement of the measured

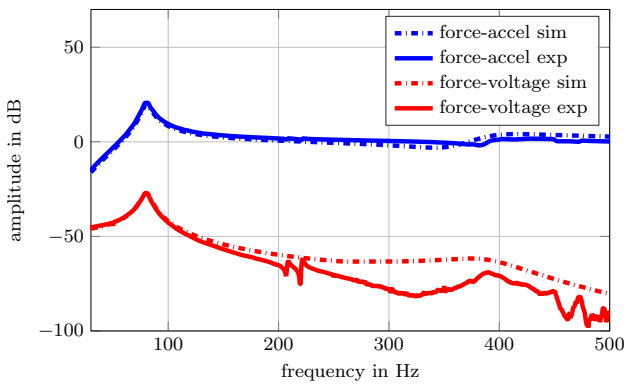

Fig. 18 Transfer functions, blue: mechanical-mechanical, red: mechanical-electrical

and simulated curves can be achieved however in the higher frequency range the measured mechanical-electrical transfer function shows a lower amplitude than the simulated one. An interesting effect is furthermore perceived by the emerging peaks between 200 and 150 Hz only in the measured mechanical-electrical transfer function. These can be explained by local asymmetric vibration modes of the plate, that cannot be observed in the mechanical transfer function because of the centred position of the sensor. Furthermore the aluminium-plates cannot be placed in the setup perfectly symmetrical like in the simulation. In the frequency range up to 200 Hz the simulations based on the developed material model show a good agreement with experimental results. Therefore numerical methods will be further used in future works to determine the electrical power-output when applying ferroelectrets to more complex models of aircraft-components. For the case of the assumed strain amplitude in the winbox (Fig. 1) a power output of around $3.6 \cdot 10^{-13}$ W is calculated using Eq. 7, which is very low since the material is used in its 31-mode. However by using a simple transmission as shown in Fig. 19 to convert the in-plane strain of the host structure into a compression of IXPP-sheets in 33-mode the power output is increased tremendously.

This is firstly due to the strain increase in the material and secondly due to the much higher δ_{33}-coefficients. The transmission of in-plane strain S_1 to the strain in the ferroelectret S_3 is calculated by

$$S_3 = -\frac{\delta y}{H} = -\frac{S_1 l_{\text{mech}} \cot(\alpha)}{Nt} = -\frac{S_1 l_{\text{mech}}^2}{N^2 t^2} \tag{17}$$

Using a realistic transmission ratio of 1/20 (i. e. an angle of 2.9°) with a projected mechanism length of 0.1 m a strain S_3 of 0.018 mm^{-1} results. Mechanical losses are neglected due to the high compliance of IXPP compared to the metallic structures. With a stack of 15 IXPP-sheets with a respective surface area of 1 cm^2 the power output is increased to 4.2 µW using Eq. 7. Although IXPP-ferroelectrets have much lower δ_{31}-constants compared to typical piezoelectric materials (Table 4), they can effectively be used for energy harvesting in bending host structures.

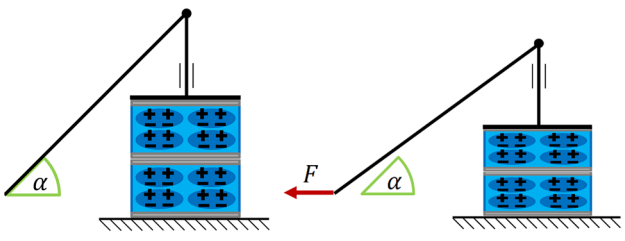

Fig. 19 Principle of an energy harvester with transmission mechanism in undeformed and deformed state. The angle α determines the transmission ratio

Table 4 Material properties for energy harvesting (*for wood materials this corresponds to the d_{14}-constant; **for wood materials this corresponds to the d_{25}-constant)

	Red beech	IXPP	PIC 255	PVDF [9, 16, 17]
Y_1 in GPa	1.334	0.133	71.79	3
Y_3 in GPa	1.334	0.0011	91.24	10
Density in kg/m^3	680	480	7800	1790
Charge constant d_{33}* in pC N^{-1}	0.044	400	394	−33
Charge constant d_{31}** in pC N^{-1}	−0.044	−0.252	−174	23
Rel. permittivity $\epsilon_{33,r}$ in –	2.3	2.16	1750	10
FOM $d_{33}g_{33}$ in TPa^{-1}	$1 \cdot 10^{-4}$	8370	13.44	−10.89
FOM $d_{31}g_{31}$ in TPa^{-1}	$1 \cdot 10^{-4}$	0.003	2.6	5

4 Conclusion

Alternative piezoelectric materials for Energy Harvesting on vibrating aircraft structures were presented in the form of biogenic wood materials with load-bearing properties and a high eco-efficiency and ferroelectrets with remarkable structural flexibility and high piezoelectric transducer coefficients. For both materials the piezoelectric effect was registered with a respective experimental setup. For wood materials the assumptions from the literature were confirmed with a determined charge constant of $\delta = 0.044$ pC/N. The low piezoelectric charge constant of wood complicates energy harvesting. The lightweight potential of wood, which enables the substitution of existing load-bearing structures, can compensate for this disadvantage. The test setup and the measurement chain were verified for wood materials with regard to environmental disturbances. An initial specimen geometry was defined for the material characterization. Compression tests were performed on wood samples with a grain angle of 45° to the direction of loading. Young's Modulus and the yield strength were determined. Investigations on different wood species under variation of the parameters will follow in future works. From this, specific values will be derived to describe the dynamic electro-mechanical performance of the transducer materials. Approaches for normative test methods will be developed to standardize the procedure. After selecting a potential material and the optimal geometry, structural integration will follow. For ferroelectrets it was shown, that the static and dynamic modelling for small structural strains of host structures is possible with linear material models, that are also used for piezoceramics. The material parameters for the model were derived from manufacturer data, capacitance measurements and by means of a tensile test. Furthermore a preliminary design of a dynamic four-point flexural test for the investigation of IXPP-ferroelectrets glued on aluminium plates was used to create an electromechanical numerical model. Finally the model was validated with measurements from an experimental test setup regarding its mechanical and electromechanical transfer functions. In the frequency range up to 200 Hz the simulations based on the developed material model showed a good agreement with experimental results. Despite not being designed for the use in 31-mode the investigated IXPP-ferroelectret showed a charge constant of $\delta_{31} = 0.252$ pC/N. This work represents the first step for the dynamic modelling of ferroelectrets attached to surfaces, without the aim of maximizing the electrical power output. In future works, optimizations regarding the ferroelectret material and the geometry of the EH will be in focus of research, as well as their experimental validation. A concept of a lightweight energy harvester design was introduced to compensate for the disadvantage of low d_{31}-coefficients, by converting the in-plane strain energy to a perpendicular compression of a ferroelectret stack. First power estimations of a specific mechanism nad a stack with a surface area of 1 cm^2 showed a power output of 4.2 µW. Furthermore the modelling approach will also be used for wood materials. For both material kinds the electrical power-output subject to more realistic load conditions in aircraft structures will be calculated and optimized using more complex numerical models. The simulations will further be validated on simplified demonstrator components.

Acknowledgements A special thanks to Prof. G. M. Sessler from the group of Electroacoustics at the Technical University Darmstadt for his consultation regarding ferroelectrets.

Funding Open Access funding enabled and organized by Projekt DEAL. Research was supported by the Federal Ministry of Economic Affairs and Energy (BMWI), Germany.

Supported by:

on the basis of a decision
by the German Bundestag

Code availability Software applications (ANSYS, MATLAB) were used and complemented with custom code.

Declarations

Conflict of interest The authors declare no conflict of interest.

References

1. Bundesverband derDeutschenLuftverkehrswirtschaft: Klimaschutz im Luftverkehr: analyse der Klimaschutzinstrumente im Luftverkehr zur CO2-Reduktion. https://www.bdl.aero/de/publikation/ analyse-der-klimaschutzinstrumente-im-luftverkehr- zur-co2-reduktion/
2. Holzmann, H., Schmelz, J., Atzrodt, H., Park, Y.J.: Demonstration of energy harvesting with piezoelectrets in aircraft structures with a simplified structure based on a NASA wingbox model. In: Proceedings of ISMA2020, pp. 2763–2774 (2020)
3. Rivers, Melissa: NASA common research model. https://commonresearchmodel.larc.nasa.gov/
4. Ross, R.J., Kan, J., Wang, X., Blankenburg, J., Stockhausen, J.I., Pellerin, R.F.: Wood and wood-based materials as sensors—a review of the piezoelectric effect in wood (2012)
5. Fukada, E.: Piezoelectricity as a fundamental property of wood. Wood Sci. Technol. **2**, 299–307 (1968)
6. Zhang, X., Wang, X., Huang, J., Xia, Z.: Quasi-static and dynamic piezoelectric d 33 coefficients of irradiation cross-linked polypropylene ferroelectrets. J. Mater. Sci. **44**(10), 2459–2465 (2009). https://doi.org/10.1007/s10853-009-3312-3
7. Zhang, X., Pondrom, P., Wu, L., Sessler, G.M.: Vibration-based energy harvesting with piezoelectrets having high d31 activity. Appl. Phys. Lett. **108**(19), 193903 (2016). https://doi.org/10.1063/1.4948649
8. Bauer, S., Gerhard-Multhaupt, R., Sessler, G.M.: Ferroelectrets: soft electroactive foams for transducers. Phys. Today **57**(2), 37–43 (2004). https://doi.org/10.1063/1.1688068
9. Zhang, X., Pondrom, P., Sessler, G.M., Ma, X.: Ferroelectret nanogenerator with large transverse piezoelectric activity. Nano Energy **50**, 52–61 (2018). https://doi.org/10.1016/j.nanoen.2018.05.016
10. Xue, Y., Zhang, X., Zheng, J., Liu, T., Zhu, B.: Comparative study of transducers for air-borne sound based on normal and irradiation cross-linked polypropylene piezoelectret films. IEEE Trans. Dielectr. Electr. Insul. **25**(1), 228–234 (2017). https://doi.org/10.1109/TDEI.2018.006492
11. Pondrom, P.: Elektret- und Piezoelektret-Wandler für Körperschallaufnahme und Energy-Harvesting, Technische Universität Darmstadt, Dissertation (2018)
12. Niemz, P., Lühmann, A., Wagner, J.: Orientierende Untersuchungen zur Ermittlung ausgewählter piezoelektrischer Konstanten an Holz. Holz als Roh- und Werkstoff **50**(12), 484 (1992)
13. Goga, V., Hučko, B.: Phenomenological material model of foam solids. Strojnícky casopis J. Mech. Eng. **65**(1), 5–20 (2015). https://doi.org/10.1515/scjme-2016-0001
14. Wu, L., Zhang, X., Zhang, X.: Mechanical and piezoelectric performance of cross-linked polypropylene films treated with extending. Ceram. Int. **41**, S218–S222 (2015). https://doi.org/10.1016/j.ceramint.2015.03.243
15. Kranz, B.: Berichte aus dem IWU. Bd. 65: Beitrag zur numerischen Beschreibung des funktionellen Verhaltens von Piezoverbundmodulen: Zugl.: Chemnitz, Techn. Univ., Diss., 2012. Auerbach: Verl. Wiss. Scripten (2012). ISBN 978-3-942267-52-6
16. Ohigashi, H.: Electromechanical properties of polarized polyvinylidene fluoride films as studied by the piezoelectric resonance method. J. Appl. Phys. **47**(3), 949–955 (1976). https://doi.org/10.1063/1.322685
17. Sappati, K.K., Bhadra, S.: Piezoelectric polymer and paper substrates: a review. Sensors (2018). https://doi.org/10.3390/s18113605